ELSEVIER

Contents lists available at ScienceDirect

Journal of Catalysis

journal homepage: www.elsevier.com/locate/jcat



Research article



An efficient approach to compartmentalize double layer effects on kinetics of interfacial proton-electron transfer reactions

Naveen Agrawal, Andrew Jark-Wah Wong, Sharad Maheshwari, Michael J. Janik *

Department of Chemical Engineering, the Pennsylvania State University, University Park, PA, USA

ARTICLE INFO

Keywords:
Electrocatalysis
DFT
Activation barriers
EDL
Electric fields

ABSTRACT

Activation barriers for elementary electrochemical reactions can show strong dependence on the composition and structure of the electrode–electrolyte interface, the electrochemical double layer (EDL), due to the highly polar nature of ion/electron transfer transition states. A compartmentalized analytical framework, built upon DFT calculations, is developed to consider complex interactions between reaction intermediates and the EDL. The approach analytically captures how altering interfacial properties, such as the dielectric constant or distribution of electrolyte charges, impact electrocatalytic activation barriers. Dipole moment changes along the reaction path plays the largest role in dictating the extent to which interfacial properties impact elementary electrochemical kinetics. The compartmentalization and uncertainty quantification capability of the developed framework is illustrated employing a Helmholtz model with two parameters, dielectric constant and double layer thickness. The framework translates routine DFT analysis of (water-assisted) hydrogenation activation barriers to proton-coupled electron transfer barriers that depend analytically on electrode potential and EDL properties.

1. Introduction

Electrocatalytic transformations contribute to sustainable energy processes by facilitating conversion between chemical and electrical energy. The development of electrochemical processes depends on the identification of catalytic materials that can provide active and selective chemical transformation paths. Significant efforts have been devoted to find electrocatalysts for CO2 reduction to hydrocarbons [1], electrochemical ammonia synthesis [2], and biomass conversion to fuels and chemicals [3-5]. Part of the challenge in discovering optimal electrocatalysts is the inability to theoretically predict the kinetics of electrocatalytic reactions. Ab-initio calculations using density functional theory (DFT) have played a significant role in the determination of reaction mechanisms to guide rational catalyst design as well as in rapid screening of catalytic materials for thermochemical conversions [6]. However, the explicit incorporation of electrolyte species and charge separation at the electrochemical interface cannot properly consider the ensemble of structures at the DFT level of theory, challenging the ability to use DFT methods to provide insight into electrocatalytic processes [7,8]. DFT-based approaches for electrocatalytic reaction energetics require simplifying assumptions of the electrochemical double layer (EDL) [9-12].

The Computational Hydrogen Electrode (CHE) formalism is a convenient and computationally efficient approach to determine the elementary electrochemical reaction free energy for a proton-electron transfer reaction [13]. This approach is often paired with the determination of the limiting potential at which all elementary steps in a mechanism have a favorable reaction free energy [10,14], and thus predicts catalytic performance using the surface binding energies and reaction free energies of key intermediates. However, the CHE formalism has key assumptions that break down when considering complex electro-catalytic reaction mechanisms [15]. The combination of the CHE and limiting potential approaches relies on a presumed universal correlation between the activation barriers and reaction energies among all elementary steps in a reaction mechanism and among all catalytic materials considered [16]. However, it is well established that the slopes and intercepts of such Bronsted-Evans-Polanyi (BEP) correlations vary between types of reactions (for example, between C-H and O–H breaking reactions [17]) or among dissimilar catalysts [15,18]. Moreover, the stronger sensitivity of charge-separated transition states to properties of the EDL, relative to stable equilibrium states, can further break the scaling relationships between the activation barriers and reaction energies [19]. Thus, approaches for the DFT evaluation of elementary electrochemical step barriers are needed to better capture

E-mail address: mjanik@psu.edu (M.J. Janik).

^{*} Corresponding author.

the role of EDL on kinetics and provide further capabilities in computational electrocatalyst design.

Capturing the impact of EDL on the activation barrier of an elementary electrochemical reaction involving proton and electron transfer is a daunting task for DFT calculations. This is due to difficulty in modeling two complex features of the interface critical to the rate of an ion transfer reaction: 1) representing the proton (ion) in a liquid/polymer electrolyte and the dynamics associated with its solvation and 2) representing the charge separation in the EDL at the electrode–electrolyte interface. Though these same modeling challenges exist when considering elementary reaction energies, representing transition states and activation barriers is more challenging due to the explicit involvement of the electrolyte in ion transfer.

Another challenge to DFT evaluation of electrochemical reaction barriers is the need to compare states along a reaction path at a constant effective electrode potential. Typical DFT calculations for electrochemical reactions are simulated with a constant system charge (typically neutral) due to the periodic nature of the unit-cell and an inability to efficiently capture the counter-ions to balance the charged systems. Constant charge calculations lead to change in work-function as an electron—ion transfer reaction progresses [20–23]. As the work-function is indicative of the effective electrode potential within the DFT model, this shift in work-function indicates the reaction energetics are not being evaluated at constant potential, limiting their relevance to experimental electrokinetic behavior. Electrochemical experiments control the electrode's potential (work-function) by compensating the excess charge on the catalytic surface through the presence of a potentiostat and the rearrangement of counter-ions in the double layer.

The potential (work-function) of the DFT simulated surface can be maintained constant along a reaction coordinate by allowing addition/removal of ions (or electrons) from the double layer (or surface) using a grand-canonical simulation [24–26]. However, a major limitation in this approach (and others that will be reviewed in Section 1.1) is that it embeds choices of how countercharges are distributed in the interfacial region, which is typically unknown for any particular electrochemical system. Moreover, the highly polar transition states can interact strongly with the separated charges (electrolyte ions and charge on electrode surface) in the EDL, increasing the impact of often arbitrary modeling choices on results.

Here we develop an analytical approach to evaluating EDL effects on electrocatalytic reaction energetics that makes explicit the dependence of energetics on EDL dielectric properties and charge distribution. Before developing this approach, we first review prior approaches to examining electrocatalytic activation barriers within DFT methods.

1.1. Current DFT approaches to elementary electrochemical reaction barriers

Recent theoretical work has attempted to address the abovementioned challenges in using DFT when approximating electrochemical reaction barriers. The three general current approaches for using DFT methods to estimate electron/ion transfer barriers are (1) explicit AIMD, (2) a built-in continuum EDL model, and (3) extrapolation approaches.

Ab-initio molecular dynamics (AIMD) can dynamically sample reaction paths with the explicit inclusion of ions (protons), solvent, and charge separation within the DFT representation. A constant work-function/electrode potential can be maintained through the grand-canonical simulation of the interface [24,27–29]. AIMD has two key limitations that inhibit its usefulness for electrocatalysis. First, approaches that maintain constant work-function by varying the electrode charge typically use homogeneous background charges or presumed counter ion distributions. Such approaches dictate EDL properties in what can be unphysical [30], compromising the advantages of using AIMD to provide a representative ensemble of structures that would be present. Second, AIMD is incredibly computationally inefficient in

capturing both rare reaction events and the distribution of slowly relaxing solvent/ions (if explicit ions are included) in the EDL region. AIMD simulations capturing the distribution of water structures at metal surfaces require months of simulations using 10's to 100's of processors [31,32]. The large correlation length and time scales of the electrolyte near the electrode surface, requiring simulations of (at minimum) 10's to 100's of nanoseconds, simply cannot be reached with AIMD. AIMD can accelerate sampling of reaction coordinates to an extent by incorporating *meta*-dynamics, but still remains limited by insufficient sampling of the electrolyte ensemble of structures [33].

Continuum EDL models provide a relatively computationally efficient alternative to AIMD by simplifying the description of the EDL [9]. Electrolyte continuum models use a presumed classical model for the distribution of electrolyte charge, often presuming a Poisson-Boltzmann (PB) distribution of electrolyte charge, that maintains the constant potential along the reaction path by varying the number of electrons/ions. Solvent properties can be represented with a continuum dielectric that interacts with the DFT region and screens the interaction between the DFT region and the classical countercharge [24,34-36]. A major limitation in these models is the (arbitrary) parameterization, as the dielectric properties and electrolyte charge distribution are not known and vary with electrode and electrolyte composition and structure. The DFT results obtained with such models can depend strongly on these arbitrary choices, however, quantifying such dependence requires repeating expensive DFT calculations with varying parameters, and is often not reported.

Extrapolation approaches are a group of DFT electrocatalysis models that do not attempt to directly include electrode potential control within the AIMD or DFT calculation. Extrapolation approaches instead use "standard" constant-charge DFT calculations with post-processing to convert them to provide potential-dependent electrocatalytic reaction energetics. Rossmeisl et al. [23] developed a cell extrapolation scheme that employs several constant-charge calculations with increasingly larger simulation cells to extrapolate the reaction energetics to infinite cell limit (constant work-function). Such cell extrapolations change the number or concentration of ions to simulate a different potential at the infinite cell limit. This extrapolation can be computationally demanding, and remains sensitive to presumed ion distributions. Chan et al. [22,37] developed a charge extrapolation scheme that precludes the demanding need to simulate constant-charge calculations with progressively larger cells and at different ion concentrations. Their method assumes a capacitive relationship between the charge on the electrode surface and the electrode potential. This relationship allows extrapolation of a barrier from a single constant charge calculation to different potentials.

Both of the extrapolation approaches presented above include significant disadvantages that are improved upon in the method presented here. Cell extrapolations [23] require explicitly varying the concentration of ions and with presumed distributions, making them expensive to consider multiple unit cell sizes and sensitive to ion distributions explicitly in the DFT model. The charge-extrapolation approach by Chan et al. [22,37] has key limitations based on presumed assumptions between charge distribution and work-function shifts (discussed later in Section 3.4). Our group previously reported approaches to extrapolate constant-charge calculation of hydrogenation activation barriers to give potential-dependent activation barriers [12,38–41]. In this approach, however, the effect of potential was considered in terms of an unknown assumed symmetry factor.

Our approach herein builds on these prior extrapolation techniques, building a more physically useful extrapolation based on interfacial dipole moments and polarizabilities. These parameters capture the leading terms in the interaction between states along the reaction path and the EDL. This allows us to create an analytical framework, at effectively no computational cost, to analyze the impact of EDL properties on electrochemical activation barriers. The "compartmentalized" framework presented allows researchers to build in individual features

of EDL interactions (solvation, interfacial field interactions, compensation for workfunction shifts along a reaction path) and quantify their impact on potential-dependent activation barriers.

1.2. Objectives of this study

We introduce a variant of the above-discussed extrapolation approaches that adds explicit consideration of the impact of EDL properties on activation barriers. Our approach builds on the charge-based extrapolation method developed by Chan et al. [22,37] by also using a single constant-charge reaction path evaluation to extrapolate potential-dependent activation barriers. We differ from the Chan approach in using the surface dipole moment and explicit work-function calculations rather than surface charge densities to quantify changes in work-function along the reaction path. We show that atomic surface charges do not accurately capture work-function variations. Instead, surface dipole changes along the reaction path are a robust predictor for variations in work-function. Overall, our approach allows facile prediction of how solvation and EDL properties impact computed activation barriers, at the computational cost of standard non-electrochemical elementary step barriers.

We model electrocatalytic kinetics of an elementary proton (ion)-electron transfer step using a combined DFT, continuum solvation, and classical double layer theory model. A micro-solvated DFT model of the local reaction center is used to model bond breaking/forming events, allowing for isolation of specific solvation effects. A few explicit water molecules capture specific solvation and a continuum solvation model (VASPSol [36,42]) captures long-range solvation effects. A classical electrostatic model (Helmholtz double layer) analytically adds (post-DFT) the impacts of electrification on reaction energetics. An advantage of our approach is the separation of electrification and solvation contributions that can simplify the quantification and demarcation of uncertainties associated with assumptions in the EDL model without repeating DFT calculations. We refer to our approach as "compartmentalized" as individual aspects of the EDL are added sequentially to our model, allowing examination of how each impacts reaction energetics.

The compartmentalized model is applied to the elementary reduction of adsorbed NH* to adsorbed NH₂* on the Rh (111) surface. This step is relevant to N2 electro-reduction to NH3, with an appreciable activation barrier [15] and significant sensitivity to EDL properties. We test the sensitivity of electrification effects to a variety of model choices: selection of the local reaction path, size of the unit cell, continuum solvation parameters, and the parameters of the double layer model (ε_r and d). We show that the change in the value of interfacial dielectric constant (ε_r) from 78 (bulk-water) to ~2 (a reasonable value for interfacial water [43,44]) can alter the reaction rate by three orders of magnitude. This illustrates the large sensitivity of the DFT-approximated electrochemical activation barriers to EDL properties, representing both a challenge to high fidelity DFT calculations and illustrating the opportunities to use an electrolyte's interfacial properties to impact electrocatalytic rate. We also contrast the NH* reduction step to an elementary step with a small dipole-change along the reaction coordinate (O* reduction to OH* on Rh (111) surface).

2. Computational methods

2.1. Electronic structure calculation

Electronic structure calculations were performed using the Vienna Ab initio Simulation Package (VASP) [45,46], a plane wave basis set pseudo-potential code. We used the projector augmented wave (PAW) method to represent the valence electron wavefunctions [37,47]. The exchange and correlation energies were calculated using the Perdew, Burke, and Ernzerhof (PBE) functional described within the generalized gradient approximation (GGA) [48]. The semicore p-type states were not considered for Rh atoms. A plane-wave basis set cutoff energy of 450

eV was used. For all calculations, dipole corrections were added in the direction normal to the surface to correct for spurious dipole interaction between the repeating unit cells. The ionic convergence limit was set to $0.03~{\rm eV}~{\rm Å}^{-1}$ while the electronic convergence limit was set to $10^{-5}~{\rm eV}.$ The Fermi level was smeared with the Methfessel-Paxton scheme [49] using a smearing width (σ) of $0.2~{\rm eV}$ for surfaces and $0.003~{\rm eV}$ for isolated molecules. Transition states were located using the Climbing Image Nudged Elastic Band method (CI-NEB) [50] with 4 to 9 images or the Dimer method [51]. Transition states were required to have atomic forces less than $+0.03~{\rm eV}~{\rm Å}^{-1},$ and vibrational frequency calculations were performed to confirm the first order saddle point.

2.2. Surface slab construction

Surface slab models of various size (3X3, 4X4, and 5X5) were used to construct periodic surfaces of Rh (111) using an experimental bulk lattice constant of 3.80 Å. The slab models were comprised of 4 layers of metal atoms. For calculations with no continuum solvation, a vacuum region of $\sim\!15$ Å was inserted between the slabs. For calculations employing continuum solvation, a vacuum region 10 times the Debye length, i.e. $\sim\!30$ Å, is inserted. Selective dynamics was implemented, and the top two layers of the slab were allowed to relax until the force convergence was achieved, while the bottom layers were fixed to imitate their bulk arrangement. The sampling of the Brillouin zone for all surface cells was conducted with a k-point mesh of 5 \times 5 \times 1 generated automatically using the Monkhorst-Pack method [49].

3. Estimation of potential-dependent activation barriers

We present a workflow to calculate potential-dependent activation barriers while incorporating adsorbate-EDL interactions using a combination of micro-solvation, continuum solvation, and EDL theory. First, in Section 3.1, we introduce our "base" model for locating a transition state within a local reaction path involving the surface, adsorbate, and a few explicit solvent molecules to model micro-solvation. Subsequent sections detail how extended solvation effects are considered, the computed barrier is assigned to a specific potential, and an EDL model then used to allow extrapolation of the barrier as a function of electrode potential. In Section 3.2 we describe how we incorporate long range solvation effects. Section 3.3 introduces a potential dependence model without EDL consideration. In Section 3.4, the charge extrapolation approach and its limitations are outlined. In Section 3.5, we directly address the limitation in charge-extrapolation by introducing a new "dipole-moment extrapolation". In Section 3.6, we analytically derive expressions for potential-dependent activation barriers with varying incorporation of electrification effects within a dipole-extrapolation approach.

3.1. Model of the reaction path and micro-solvation

Our goal is to identify a local representation of the transition state for the transfer of a proton/electron pair to an adsorbed species (A^*) to form an adsorbed product (AH^*) for the elementary reaction:

$$A^* + H^+(aq) + e^- \leftrightarrow AH^* \tag{1}$$

 A^* and AH^* can include explicit water molecules $(A(H_2O)_n^*)$ in a microsolvation representation of the adsorbed species. Though the CHE model provides an approach to reference the energy of the H^++e^- pair from their "bulk reservoir," modeling the reaction path requires including the proton within the unit cell. Fig. 1 shows a proposed local model of the reaction path for proton transfer that includes an initial state with the proton included as a surface adsorbed H species, and identifies a saddle point on the potential energy surface involving A-H bond formation with the assistance of explicit H_2O .

The potential energy surface (PES) is sampled by first optimizing an

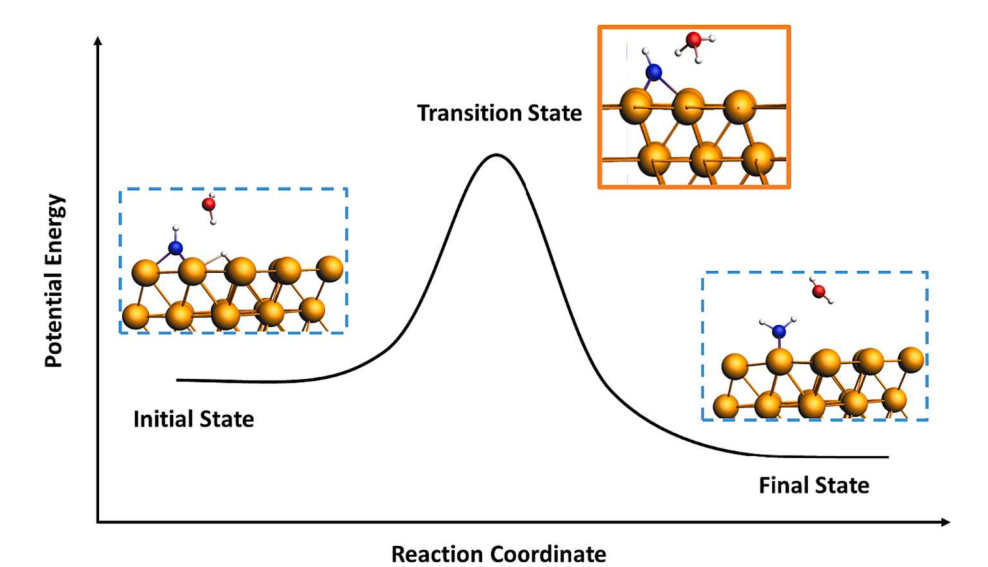


Fig. 1. One-dimensional graphical overview of the local reaction path for transfer of H^* to A^* (initial state) to form AH^* (final state). Example given is for NH^* reduction to NH_2^* on Rh (111). A single explicit H_2O molecule is included to represent micro-solvation. Atom colors are depicted as orange = Rh, N = blue, O = red, and H = white. (For interpretation of the references to color in this figure legend, the reader is referred to the web version of this article.)

"initial state" with an H atom adsorbed near A* and a "final state" where H is transferred to form AH*. Both states include $n=0,\,1,\,$ or 2 explicit H_2O molecules to model the micro-solvation interaction. A saddle point is then located on the PES for A-H formation using the CI-NEB [50] and DIMER [51] search tools. The PES is complex when considering a combination of an adsorbate (NH* for most of the discussion in this work), water molecules, and a transferring H*. As a result, there may be multiple saddle points on the PES that involve H transfer, and we cannot assure the specific saddle point located represents the minimum energy path for A* reduction to AH*. Therefore, the located saddle point provides an upper bound on the energy of the transition state, as a more preferred path could only offer a lower barrier.

With a transition state located, we can now consider how to develop a potential-dependent activation barrier for the reaction given in Eq. (1).

The activation barrier for the reaction $(\Delta G_{act}(U))$ is the free energy of the transition state at some potential $U(G_{TS}(U))$ relative to the combined free energies of the reactants (A^*, H^+) in the bulk electrolyte, and the e-) at the same potential:

$$\Delta G_{act}(U) = G_{TS}(U) - G_{A^*}(U) - G_{H^+(bulk)} - G_{e^-}(U)$$
(2)

Using the CHE approach [13], the free energy of the proton/electron pair is replaced with the free energy of hydrogen gas, and the potential U is then explicitly expressed on the reversible hydrogen electrode (RHE) scale:

$$\Delta G_{act}(U_{RHE}) = G_{TS^*}(U_{RHE}) - G_{A*}(U_{RHE}) - \frac{1}{2}G_{H_2} + |e|U_{RHE}$$
(3)

The activation barrier is converted from the RHE scale to a standard hydrogen electrode (SHE) scale in Eq. (5) through a well-known conversion as shown in Eq. (4).

$$|e|U_{RHE} = |e|U_{SHE} - 0.0591pH \tag{4}$$

$$\Delta G_{act}(U_{SHE}) = G_{TS^*}(U_{SHE}) - G_{A^*}(U_{SHE}) - rac{1}{2}G_{H_2} + |e|U_{SHE} - 0.0591pH$$
 (5)

This work considers potentials on the SHE scale since the discussion focuses on corrections to constant potential and reference to the potential of zero charge. Free energies (G) of surface bound species (ex: A^*) in Eq. (5) are calculated by implementing zero-point energy (ZPE) and entropic corrections on DFT calculated energies (E).

$$G_{A^*} = E_{A^*}^{DFT} + E_{A^*}^{ZPVE} - S_{A^*}^{Vib}T$$
 (6)

Free energy of $\rm H_2$ (g) is determined using the ideal gas approximation and statistical mechanics corrections to a pressure of 1 atm. A temperature of 300 K is used for the entropic vibrational corrections. Eq. (5) provides a base model to approximate the activation barrier for A-H* bond formation at a specific potential on the SHE scale and pH. This base model approximates that the transition state occurs after electron transfer is complete, making the slope of the barrier with potential equal to |e| (a symmetry factor of 1). This approximation is not universally (or typically) valid for elementary proton-electron transfer steps. The "corrections" presented in Sections 3.5 and 3.6, adjusting relative DFT energies to a constant potential formalism and including EDL interactions, build upon Eq. (5) and remove the assumption that electron transfer is complete at the transition state.

3.2. Incorporating long-range solvation

Section 3.1 considers solvation of only 1 or 2 explicit water molecules along the reaction coordinate. Eq. (5) is modified to incorporate long range solvation represented by $\Delta\Delta G_{sol}$. For simplicity, here and onwards, the pH term is dropped to consider pH=0, and potentials (U) are defined to be on an SHE scale.

$$\Delta G_{act}(U) = G_{TS^*}(U) - G_{A^*}(U) - \frac{1}{2}G_{H_2} + |e|U + \Delta \Delta G_{sol}$$
(7)

$$\Delta \Delta G_{sol} = \Delta G_{TS^*,solv} - \Delta G_{A^*,solv} \tag{8}$$

where $\Delta\Delta G_{sol}$ is the solvation free energy change between the reactant and transition state due to the presence of extended solvent near the reaction center not captured in the micro-solvation. $\Delta\Delta G_{sol}$ can be approximated by using either continuum solvation approaches or molecular dynamic approaches. Here, VASPSol (continuum solvation model in VASP [36,42]) is used to quantify $\Delta\Delta G_{sol}$. The solvation energy of each surface bound species ($\Delta G_{A^*,solv}$) in Eq. (9) is estimated by taking the difference between the free energy of the micro-solvated initial or transition state with VASPSol implemented relative to the free energy of the same species without VASPSol implemented:

$$\Delta G_{A^*,solv} = \left[E_{A^*}^{DFT,VASPSol} + E_{A^*}^{ZPVE,VASPSol} - S_{A^*}^{Vib,VASPSol} T \right] - G_{A^*}$$
(9)

where the left bracketed terms are the free energy of solvated A* obtained from VASPSol with the ZPE and entropic corrections. The reliability of such continuum solvation approaches to represent solvation about an electrode-aqueous electrolyte interface is not established, and we investigate the dependence of the differential solvation energy on continuum solvation parameters (dielectric constant). We approximate that both the explicit (micro-solvation) and continuum solvation contributions are potential independent.

3.3. Simple potential-dependent models without EDL consideration

A series of models is built including additional features of an EDL in representing the potential-dependent energies of TS* and A* $(E_{TS^*}(U) \ and \ E_{A^*}(U))$.

In the first approach (Model 1a), we neglect the variation of workfunction (potential) along the reaction path within a constant-charge calculation. We also neglect the potential dependence of surface bound species free energies. The potential independent free energy of the surface bound species is then directly calculated from DFT with ZPE and entropic corrections as described in Eq. (6) and assumed to be assigned at the work-function of the bare model surface (ie, the Rh(111) work-function for our example system). The work-function of finite size model surface does not stay fixed along a reaction coordinate in a constant-charge DFT calculations, so assigning a potential for these energies is somewhat arbitrary. However, following the assumption that work-function is unaffected by the presence of intermediates, here, we assign the DFT calculated free energies of both surface intermediates and the corresponding activation barrier at the potential of the bare model surface (without any intermediate). The potential of zero charge (PZC) of the bare model surface at an absolute scale (SHE) can be calculated from the work-function of the bare surface using Eq. (10).

$$U_{pzc} = \left(\frac{\varnothing_{bare} - \varnothing_{SHE}}{e}\right) \tag{10}$$

$$\Delta G_{act}^{1a} \left(U_{pzc} \right) = \Delta G_{act}^{o} = G_{TS^*} - G_{A^*} - \frac{1}{2} G_{H_2} + \Delta \Delta G_{sol} + |e| U_{pzc}$$
 (11)

where \emptyset_{bare} represents the calculated work-function of the bare surface and \emptyset_{SHE} is an estimate of the work-function of the standard hydrogen electrode. Please see Supplementary Section S1, and specifically Eq. (S2), for discussion of how workfunctions are calculated and their relationship to surface-normal dipole moments.

 ΔG_{act}^o represents the free energy difference between the TS* and A* $+\frac{1}{2}~H_2$ (g) (with a solvation correction) assigned at the PZC of bare surface. Using the linear dependence of the electron energy with respect to the applied potential, the potential-dependent activation barrier for Model 1a is defined as

$$\Delta G_{act}^{1a}(U) = \Delta G_{act}^o + |e|(U - U_{pzc})$$
(12)

Model 1a in Eq. (12) neglects any effect of the EDL electrification on the barrier, leading to a slope of barrier with potential of 1 | e |. We further introduce Model 1b (Eq. (13) in which we include a transfer coefficient (β) to allow for adjustment of the slope of the activation barrier with potential.

$$\Delta G_{act}^{1b}(U) = = \Delta G_{act}^{o} + \beta |e| (U - U_{pzc})$$
(13)

Model 1a is a simple approach that calculates potential-dependent barriers but arbitrability assigns a barrier to U_{pzc} as defined in equation (10) and assumes a slope of barrier with potential of 1 eV/V. While Model 1b introduces a transfer coefficient, the value of β is difficult to approximate and Model 1b provides no guidance on how to estimate this value. Models 1a and 1b are simple models that have two major limitations when predicting potential-dependent activation barriers. First, both models assume variation of the work-function along the reaction

coordinate did not impact the relative DFT energies of the initial and transition state. Second, these models either include no interaction of initial and transition states with the separated charge at the interface (1a) or provide an arbitrary estimation of such an effect using a presumed symmetry factor (1b).

3.4. Charge-extrapolation approaches and their limitations

In developing the "compartmentalized" approach, the next step is to consider how to correct computed constant-charge energies and incorporate interactions with the electrified surface-counter charge within the EDL. The approach used herein is inspired by the existing extrapolation approaches. In presenting our approach, we contrast with an existing charge-extrapolation approach proposed by Chan et al. [37].

For addressing the change in work-function along the reaction path, a charge-extrapolation approach can use a post-hoc energy correction term to extrapolate the energy of a TS^* or A^* as a function of potential:

$$G_{\lambda}(U) = G_{\lambda}(U_{\lambda}) - \int_{q=0 \text{ or } U=U_{\lambda}}^{q(U)} U(q) dq$$
 (14a)

$$G_{\lambda}(U) = G_{\lambda}(U_{\lambda}) - \frac{1}{2}C_{dl}\left(U - U_{\lambda}\right)^{2} \tag{14b}$$

In the equations (14a)-b and subsequent sections, λ is used as an index to refer to a specific state along the reaction coordinate $(\lambda = TS^* \text{ or } A^*)$. Eqs. 14(a-b) estimates the amount of capacitive charging energy required to extrapolate the energy of the adsorbed intermediate away from the PZC of state λ (U_{λ}), enabling the calculation of grand canonical free energies. Eq. (14a) calculates the total amount of work to charge the EDL integrated while moving from the potential U_{λ} to U. Eq.14a allows us to calculate the energy correction term with the knowledge of a charge-potential relationship and the PZC of the state apart from the DFT calculated energy. $E_{\lambda}(U_{\lambda})$ is the DFT calculated energy of state λ within the constant-charge calculation and $G_{\lambda}(U_{\lambda})$ adds ZPVE and entropy corrections.

Apart from DFT calculated energies, the charge extrapolation model requires the knowledge of the changes in PZC along the reaction path and the capacitance of the double layer. The PZC of the any state λ (U_{λ}) on an SHE scale is directly related to the state's work-function as shown in Eqn 15:

$$U_{\lambda} = \left(\frac{\varnothing_{\lambda} - \varnothing_{SHE}}{|e|}\right) \tag{15}$$

In theory, any expression of the capacitance can be used in Eqs. 14 to to calculate grand canonical free energies during electrocatalysis. However, the main challenge is the choice of such model, one that accurately describes the capacitance profile for a given electrocatalytic reaction. While many approaches can describe the capacitance explicitly within the simulation, Chan et al. measured the charge on the surface for different intermediate states using a parallel plate capacitor model of charge-transfer during reaction events. In their approach, the capacitance is determined as a ratio of measured change in surface charge to the measured change in the PZC (work-function) along the reaction path.

$$C_{dl} = \frac{q_{TS} - q_{IS}}{U_{TS} - U_{IS}} \tag{16}$$

We can use the relationship in Eq. (16) to describe the variation of PZC (work-function) of any state λ (U_{λ}) relative to the bare surface (U_{pzc}) which, by definition has zero-surface charge, as a function of surface charge (q_{λ}). This expression will be useful in the next section when we compare our dipole-extrapolation approach with the charge-extrapolation approach.

$$U_{\lambda} = U_{pzc} + \frac{q_{\lambda}}{C_{dl}} \tag{17}$$

The charge extrapolation approach of Chan et al. effectively uses Eqs. (14)–(17) with the assumed parallel-plate capacitor model of surface-charging to extrapolate the energy difference between initial and transition state as a function of potential.

We identify three key limitations to the charge-extrapolation approach of Eqs. (14)-(17). First is the assumed relationship between the shift in PZC (work-function) and excess surface charge due to the presence of adsorbate as described in Eqs. (16) and (17). The excess surface charge due to adsorption is caused by molecular reorganization, which does not necessarily behave like charging a parallel plate capacitor. We show in Fig. S2 (b), using a simple set of test calculations (Na adsorption on top of Pt(111) with varying distance between Na and Pt surface), that the atomic charges of a surface adsorbate cannot predict the variation in work-function. The spatial distribution of the charges (charge separation distance) also affects the work-function. Moreover, the use of charge-partitioning schemes such as Bader-charge to measure the excess surface charges additionally introduces inaccuracies in the calculation of capacitance through Eq. (16). The second issue with this approach is the assumption that changes in the electrode potential affect only the energy stored in the double layer capacitor (Eq. 14) while ignoring the interfacial interactions between the interfacial field and surface species. A third issue is that this approach provides no clear path to consider how the change in interfacial properties due to the electrolyte (ion distribution, dielectric properties, or, collectively, capacitance) alter reaction energetics. Incorporating such effects in the charge extrapolation approach would require explicitly modeling these species atomistically and measuring how they change the relationship between surface charge and work-function shift. Establishing such a relationship would suffer from the first two issues mentioned here, as well as the impracticality of sampling an ensemble of relevant structures.

3.5. Combined Helmholtz model and dipole-extrapolation approach

We address the three limitations of the charge-extrapolation approach by proposing a new extrapolation approach based on interfacial dipoles and electrochemical double layer theory rather than excess surface-charges. Surface dipoles are a robust indicator of variation of work-function [52]. Second, we describe a generalized framework to incorporate the dipole-field interactions for determining the potential-dependent energies of polar intermediates at a charged interface. Third, we use a simple Helmholtz model of the double layer, instead of explicit ions and solvent, allowing transparent analytical connection between double layer properties (charge distribution and dielectric properties) and the potential dependence of surface species energies.

We first replace the relationship between PZC and surface charges (Eq. (17) with a robust relationship between the surface dipoles and the work-function and correspondingly the PZC:

$$U_{\lambda} = U_{pzc} + \frac{\mu_{\lambda}}{\varepsilon A} \tag{18}$$

where U_{pzc} is the PZC of the bare surface, μ_{λ} is the surface normal component of the dipole moment of state λ , ε is the permittivity of the medium, and A is the area of the surface slab. Note that $\varepsilon=\varepsilon_r\varepsilon_o$ where ε_r is the relative permittivity (dielectric constant) and ε_o is the permittivity of vacuum. The surface work-function shows a perfect correlation with the surface normal dipole moments, as discussed in Supplemental Sections S1-S2. Surface charges do not capture the effect of separation between the charge and countercharge of an interfacial dipole, whereas this separation does influence the work-function. The predictive relationship between surface dipoles and surface work-function is well established in the surface science literature [20,21,53,54]. This relationship can be extended to account for the presence of a medium with the relative permittivity $\varepsilon_r = \varepsilon/\varepsilon_o$. The dielectric medium dampens the shift in the work-function by a factor [53] ε_r as can be inferred from Eq. (18). We re-emphasize that U_{pzc} in Eq.18 is the PZC (work-function put

on an SHE scale, Eq. (10) of the bare slab, such that the surface dipole moment μ_i dictates the shift in PZC of state λ .

To further approximate the potential-dependent energy of state λ (TS* or A*), dipole-field interaction terms are added to the capacitive energy term:

$$G_{\lambda}(U) = G_{\lambda}(U_{\lambda}) - \frac{1}{2}C_{dl}(U - U_{\lambda})^{2} + \mu_{\lambda}F_{\lambda} + \alpha_{\lambda}\frac{1}{2}F_{\lambda}^{2}$$
(19)

The first term on the right hand side is the free energy of the intermediate directly calculated from (neutral) DFT calculations with continuum-solvation, ZPE, and entropic contributions included. The second term represents the capacitive energy stored at a potential away from the PZC. The third term is the 1st order interaction between adsorbate and the interfacial electric field (F_{λ}) described by a dipolefield term. The final, 2nd order term represents the interaction between the field and adsorbate due to the polarizability of reaction intermediates. The surface normal dipole (μ_{λ}) and polarizability (α_{λ}) of a surface bound intermediate can be determined from neutral adsorbate/ slab calculations, as described in supplementary information (Supplemental Section S3). We next need to prescribe how to determine the interfacial electric field (F_{λ}) experienced by state λ at any given potential (U). The capacitance of the EDL was modeled using a Helmholtz model with two parameters, instead of an explicitly modeled EDL, to relate the interfacial electric field to potential. The Helmholtz model of a double layer simplifies the description of capacitance (Eq. (20a), or capacitance per surface area in Eq. (20b) using a parallel plate of hypothetical countercharge distance d away from the electrode surface and an effective permittivity of double layer ε . The primary advantage of using a Helmholtz model is the ability to quantify how the capacitance changes (calculated DFT energetics) with two simple and physical parameters, ε and d. The Helmholtz model also allows us to explicitly describe the electric field (Eq. (21)) which allows direct capture of dipole-field interactions.

$$C_{dl} = \frac{\varepsilon A}{d} \tag{20a}$$

$$\overline{C_{dl}}(\mu F/cm^2) = 8.86* \left(\frac{\varepsilon_r}{d\left(\mathring{A}\right)}\right)$$
 (20b)

The electric field is related to potential deviation from the PZC of state λ and the double layer thickness (d):

$$F_{\lambda}(U) = \frac{U - U_{\lambda}}{d} \tag{21}$$

where the sign of field is positive when the electrode surface is positively charged ($U>U_{pzc}$). Combining Eqs. (18)–(21), Eq. (22) provides a compartmentalized framework to calculate potential-dependent energies of any state λ (TS* or A*) from standard uncharged adsorbate–surface slab DFT calculations:

$$G_{\lambda}(U) = G_{\lambda}(U_{\lambda}) - \frac{1}{2} \frac{\varepsilon A}{d} (U - U_{\lambda})^{2} + \mu_{\lambda} \left(\frac{U - U_{\lambda}}{d} \right) + \alpha_{\lambda} \frac{1}{2} \left(\frac{U - U_{\lambda}}{d} \right)^{2}$$
 (22)

The free energy of state λ in Eq. (22) is dependent on (1) DFT calculations of G_λ (E_λ with ZPVE, entropy corrections, and continuum solvation if desired), the surface normal dipole moment (μ_λ which also determined U_λ through Eq. (18) and the surface normal polarizability α_λ and (2) analytically dependent on EDL properties ε and d. This contrasts with continuum or AIMD EDL approaches that provide potential-dependent state free energies, but embed parameterization of EDL properties and/or struggle to provide sufficient dynamic sampling, without easily evaluating the dependence of energetics on EDL properties or sampling. The "compartmentalized" approach used herein, however, makes the assumption capacitive charging, solvation, and interfacial field effects can be considered separable.

3.6. Estimating electrochemical activation barriers with EDL consideration

Eq. (22), combined with Eqs. (2)–(9), is used to calculate free energy differences between a transition and reactant state. Fig. 2 shows the complete form of the progressive models for estimating the electrochemical activation barriers.

Fig. 2 illustrates that each of Model 1a, 2a, 2b, and 2c build progressively additional features of how the EDL impacts the potentialdependent activation barrier. Model 1a computes the activation barrier at the PZC of the bare surface and presumes complete electron transfer at the transition state, as presented in Sections 3.1-3.3. Model 2a adds the capacitive corrections to correct the constant charge activation barriers to a constant potential. Model 2b adds adsorbateinterfacial electric field interactions, and Model 2c adds second order polarizability-field interactions. Model 1b (Eq. (13)) is not included in Fig. 2 as it is not within the progression of adding features, and instead adds an arbitrary correction of the symmetry factor. Each of the "correction" terms added progressively in Models 2a-c include terms that depend on the unit cell area, which we refer to as "finite cell" terms. The majority of these terms are potential independent. Each of Models 2a-c includes terms that are strongly potential-dependent, which we refer to as "explicit electrification" terms. Table 1 summarizes the grouping of terms into these categories.

The symmetry factor can be analytically expressed for each model by taking the derivative of the activation barrier with respect to U, as discussed in Supplementary Section S4.

4. Results and discussion

The "compartmentalized" extrapolation approach is applied to determine the potential-dependent activation barrier of NH* reduction to NH2* on Rh (111). Section 4.1 examines the impact of specific solvation, implicit solvation, and reaction path on the activation barrier, using Models 1a-b. In Section 4.2, the impact of including EDL effects on barriers is examined using Models 2a-c, with single values presumed for the EDL dielectric permittivity and countercharge distribution. In Section 4.3, the impact of reaction path on the potential-dependent barriers is revisited within Models 2a-c. In Section 4.4, the sensitivity of the predicted barriers to the size of the unit cell is examined. In Section 4.5, the sensitivity of barriers to the choice of double layer parameters $(\varepsilon_r \text{ and } d)$ is explored. In Section 4.6, the barrier for the elementary reduction of O* to OH* on Rh (111) is contrasted with NH* reduction to NH₂*, establishing the surface-normal dipole moment change along the reaction coordinate as a descriptor of the impact of EDL properties on activation barriers.

Table 1Classification of the post-DFT "correction" terms to the activation barrier added progressively across Models 2a–c.

Туре	Capacitive (2a)	Dipole (2b)	Polarizability (2c)
Finite-cell	$-\frac{1}{2}\frac{\Delta(\mu^2)}{\varepsilon Ad}$	$-\frac{\Delta(\mu^2)}{\varepsilon Ad}$	$+\frac{\Delta \left(lpha \mu^{2} ight)}{2arepsilon^{2}A^{2}d^{2}}-rac{\Delta \left(lpha \mu ight)}{arepsilon Ad^{2}}U^{'}$
Explicit electrification	$\frac{\Delta\mu}{d}U'$	$\frac{\Delta\mu}{d}U'$	$\frac{1}{2} \frac{\Delta \alpha}{d^2} U^2$

4.1. Solvation effects and variable β using Model 1

Fig. 3 shows activation barriers (ΔG_{act}^o) calculated using Model 1 at $U = U_{pzc}$. Barriers were calculated with 1 or 2 explicit water molecules included in the reaction path and with inclusion of a continuum solvation model. Structures of initial, transition, and final states are illustrated in Fig. S6. With a single water molecule assisting proton transfer, the transition state structure resembles an H₃O⁺ with one H extended to begin forming a N-H bond. The barrier at the Rh(111) PZC is 1.47 eV. Including an additional water molecule leads to concerted proton transfer in which a partial positive charge is delocalized across NH₂* and $H_5O_2^+$ as the N-H bond forms, reducing the barrier by 0.4 eV. The significant enthalpic stabilization of including an additional water would out weight the entropy loss of fixing a second water molecular at the transition state, as this 0.4 eV stabilization exceeds that of a typical O-H hydrogen bond in liquid water (~0.24 eV). We do not consider the explicit inclusion of additional water due to both the complexity of possible reaction paths and the anticipation that the enthalpic stabilization would no longer exceed the entropic loss of fixing an additional water within the reaction coordinate (the entropy loss for a single water molecule at standard conditions in the liquid phase to be fixed frozen at the transition state is 0.22eV). The inclusion of 2 explicit water molecules was also found to be sufficient in an embedding approach to model proton transfer in aqueous acid catalyzed proton transfer reactions [55].

Solvation interactions beyond the explicit 2 water molecules can be approximated with continuum solvation. Fig. 3 shows the effect of varying dielectric constant of the continuum solvation model on the calculated activation barriers. The interfacial dielectric constant for water is expected to be closer to 1 (vacuum) than 78.4 (liquid water) since interfacial water is significantly confined with dynamics altered due to proximity to the metal [43,44]. The continuum solvent better stabilizes the transition state than the reactant state, such that the barrier of 1.07 eV is reduced by $\Delta\Delta G_{sol}=0.04eV$ for $\varepsilon_r=5$ and $\Delta\Delta G_{sol}=0.15eV$ for $\varepsilon_r=78.4$. Moving forward, we use the barrier for the system (1.03 eV at $U=U_{PZC}$ for bare Rh(111) = 0.55 V-SHE) with two explicit water molecules and a continuum dielectric constant of 5 to build upon with the more complex models. As shown above, the choices made in

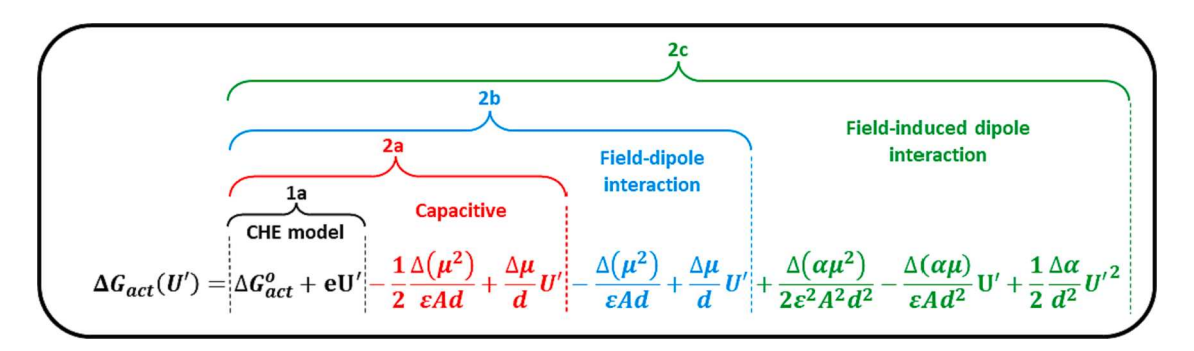


Fig. 2. Estimating electrochemical activation barriers using dipole-extrapolation approach and a Helmholtz description of the electrochemical double layer. Four different models compartmentalize the influence of EDL interactions on activation barriers: Model 1a using constant charge DFT calculations with no EDL description or correction to constant work-function, Model 2a uses a capacitive correction based on surface dipole moments to calculate the activation barrier at a constant work-function, Model 2b adds field-dipole interaction, and Model 2c adds second order field-induced dipole (polarizability) interaction. The following are model parameters used in Fig. 2: ε = permittivity of the medium, d = distance between the Helmholtz parallel charge plates, D = D

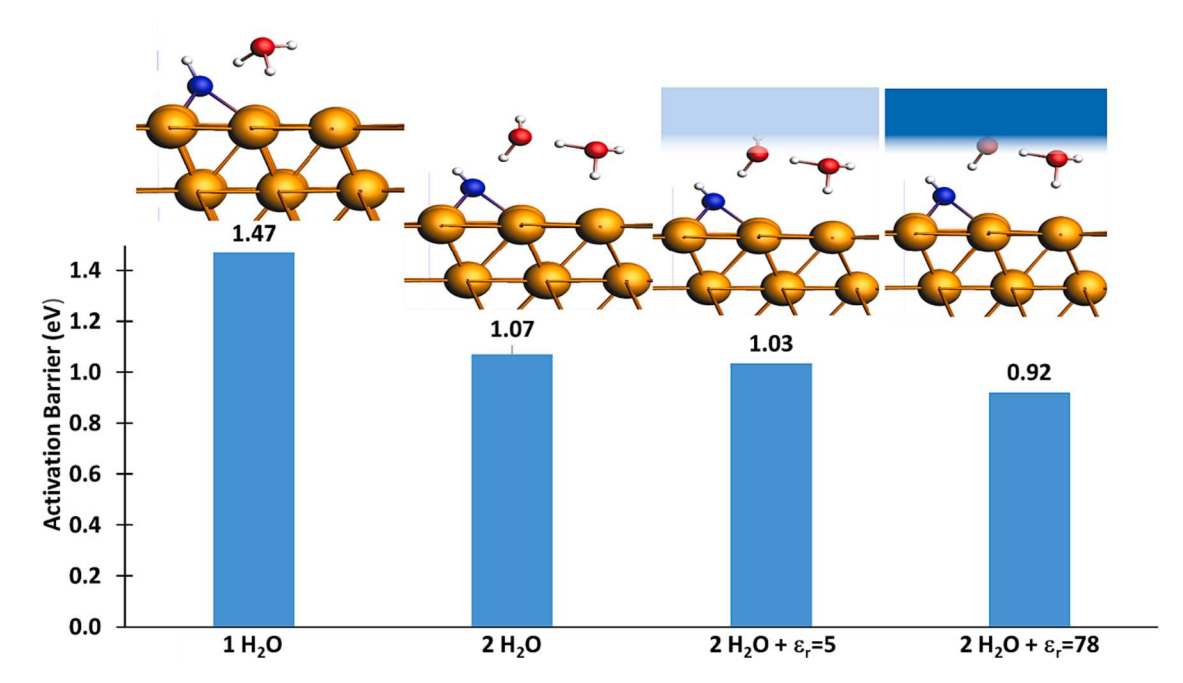


Fig. 3. Activation barriers for NH* reduction to NH₂* on the Rh(111) 3x3 surface using Model 1 (ΔG_{act}^o) evaluated at $U = U_{pzc}(0.55V - SHE)$. Insets illustrate transition state structures for NH* reduction.

explicit and implicit solvation models can cause the barrier to vary by \sim 0.5 eV, though reasonable choices reduce this variance.

Model 1a serves as the basis for building Model 2 upon, though we also consider a Model 1b (Eq. (13) in which an arbitrary symmetry coefficient is used to dictate the potential dependence of the barrier. Fig. 4 shows potential-dependent barriers using Model 1a ($\beta=1$) and Model 1b (for $\beta=0.3$, 0.5, or 0.7). As Fig. 4 illustrates, varying β between 0.3 and 0.7 causes the barrier at -0.5 V-SHE (a potential in the range of interest for N_2 reduction to NH_3) to vary by 0.3 eV. A barrier variation of 0.3 eV could cause a rate constant variation of 5 orders of magnitude at room temperature, highlighting sensitivity of DFT-predicted rates to choices in model parameters. Model 2 derives potential-dependent barriers, and therefore β , directly from the electronic structure of initial and transition states and parameters within a Helmholtz model, allowing to quantify the sensitivity of barriers to these values.

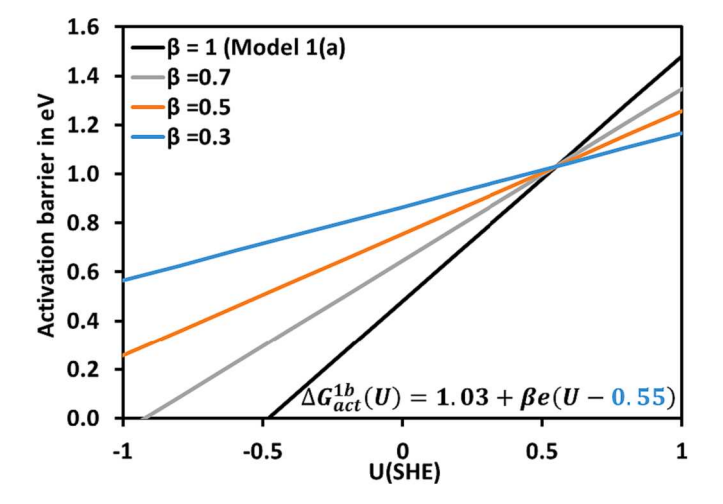


Fig. 4. Sensitivity of NH * to NH $_{2}^{*}$ reduction barrier on Rh(111) to the selection of symmetry factor with Models 1a and 1b.

4.2. Potential-dependent barriers using Model 2 with $\varepsilon_r = 5$, d = 3 Å

To include the "correction" terms of Model 2 upon Model 1a, choices must be made for the effective dielectric constant within the EDL and the Helmholtz distance of the countercharge from the surface. These values are unknown for any given system, and subsequent sections evaluate the sensitivity of computed barriers to these choices. In this section, values of $\varepsilon_r=5$ and d=3 Å are used and we examine the magnitude of the resultant "correction" terms. The value of $\varepsilon_r=5$ is consistent with that used in the continuum dielectric model of longer range solvation, though there is no inherent requirement in the approach used herein that these two values be identical. The value of d=3 Å is reasonably representative of a minimum countercharge distance that allows for a single layer of water to separate the countercharge from the surface. Using Eq. (20b), these values result in a specific capacitance of $14.8\mu F/cm^2$, which is in the range of experimentally measured specific capacitance [56,57].

Fig. 5 and Table S5 shows the potential-dependent electrification contributions to the barrier of the model reaction, separated into the individual: capacitance (Model 2a), 1st order electric field-dipole (Model 2b), and 2nd order polarizability (Model 2c) terms using expressions in Fig. 2 and Table 1. The surface normal dipole moments and polarizabilities of the reactant and transition states needed for computing the terms in Fig. 5 are given in Table S4.

Fig. 5(a) shows the 'finite-cell corrections,' which correct for the variation in work-function along the reaction path due to the use of a finite unit cell size. For the chosen set of double layer parameters and the specific NH* to NH $_2$ * reaction path, the total magnitude of finite cell corrections is approximately -0.10 eV. The color-coded column indicates both the magnitude and sign of finite-cell corrections from the individual terms in Table 1.

Fig. 5(b) shows the explicit electrification corrections determined from the cell-size independent terms evaluated from Model 2(a-c). These corrections in their analytical form are dependent on the difference between the applied potential and the PZC of the bare surface, and go to 0 at U_{pzc} . These corrections affect the potential dependence of barriers, and, therefore, the symmetry factor.

Fig. 6 shows the potential-dependent barriers for Models 1a and 2a-c using the equation in Fig. 2 and $\varepsilon_T = 5$ and d = 3 Å. Capacitive (Model 2a)

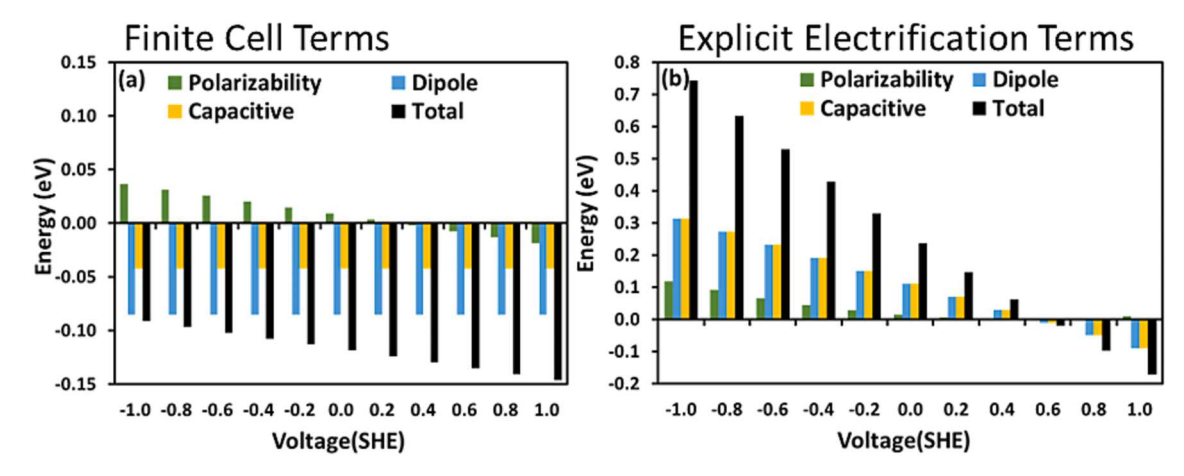


Fig. 5. Contributions to the potential-dependent barrier of NH* reduction to NH₂* on Rh(111) computed using Model 2(a-c) as compartmentalized in Table 1. (a) Potential independent or weakly dependent "finite cell size" terms (row 2 from Table 1). (b) Explicit electrification terms (row 3 from Table 1). "Capacitive" terms represent terms included in Model 2a, "Dipole-field" terms represent terms added for Model 2b, and "Polarizability" represents terms added in Model 2c. Values of ε_r = 5 and d = 3 Å are used for the Helmholtz EDL model. Negative terms reduce the activation barrier and positive terms raise the activation barrier.

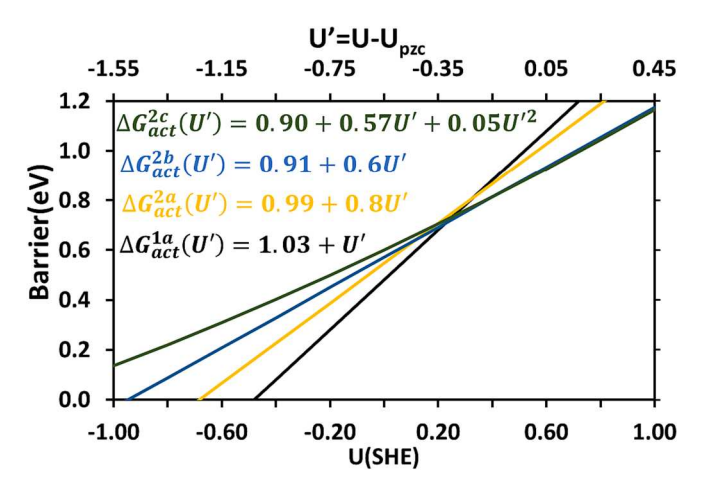


Fig. 6. Activation barrier of NH* reduction to NH₂* on Rh(111) as a function of potential (SHE scale represented on bottom x-axis, and top x-axis labeled relative to the Rh(111) PZC of 0.55V-SHE) using Models 1a and 2a-c with $\varepsilon_r = 5$ and d = 3Å. Equations representing each curve are given on the plot.

and 1st order dipole-field interactions (Model 2b) each reduce the symmetry factor by the same amount (0.20), as this reduction is given for each of these terms as the ratio of the reactant-to-transition-state dipole moment change ($-0.60e\mbox{\sc A}$) to the double layer thickness (3Å). The significant change in surface dipole moment between the reactant and transition state signifies that charge transfer is not complete at the transition state, with the NH*-H $_5$ O $_2$ complex retaining a partial positive charge. In Models 2a and 2b, this change in dipole moment leads to a reduction in the symmetry factor, consistent with the symmetry factor being indicative of the extent of charge transfer accomplished at the reduction transition state.

The second order term, arising from differences in the polarizability between the initial and transition state, has only a minor effect on the barrier unless far from the PZC. Within 0.5 V of the PZC, this term is rather negligible, though ignoring the polarizability in the potential range of interest for the nitrogen reduction reaction (-0.4, -0.8, -1V SHE) would lead us to underestimate the barrier (by 0.07, 0.13, and 0.17 eV, respectively).

4.3. Sensitivity of electrification effects to the choice of local reaction path

In section 4.1, barriers were reported with 1 or 2 explicit water

molecules involved in proton transfer to the adsorbed NH* species. Inclusion of a second water molecule lowers the activation barrier (at the PZC) by helping to stabilize the transferring proton. Inclusion of a second water molecule also leads to a more polarized transition state structure (dipole moment change of $-0.60~e^{\rm A}$ relative to $-0.21~e^{\rm A}$ for 1 explicit water), as the delocalization stabilizes a larger positive charge and a transition state "earlier" on the coupled proton-electron transfer path. These two transition states can be considered to represent two different paths, and we can use Model 2c to explore the extent to which the preferred path (ie, which transition state is lower in energy) depends on electrode potential.

Fig. 7 shows the barrier estimates including electrification corrections for 1-water and 2-water pathways. The smaller dipole moment change, lesser positive charge, and "later" transition state in the 1-water reaction path leads to a symmetry factor closer to 1. Below -1.2 V-SHE, this 1-water reaction path is preferred to the 2-water path.

This transition of favorability from the 2-water pathway to the 1-water pathway reveals both an advantage and disadvantage of the compartmentalized, extrapolation approach used herein. An advantage illustrated here is that once possible local transition state models are located, with various proton transfer trajectories and involvement of solvent, the potential dependence of their stability can be considered and the preferred path identified at any potential. However, the decoupling of modeling the reaction path and analytically including the

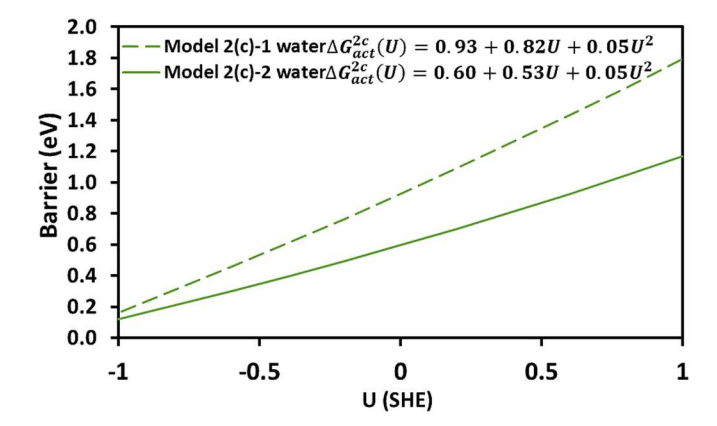


Fig. 7. Activation barrier as a function of electrode potential for NH* reduction to NH₂* on Rh(111) considering the explicit involvement of 1 (dashed line) or 2 (solid line) water molecules in proton transfer. Model 2c is used with EDL properties of $\varepsilon_r = 5$ and d = 3Å.

potential dependence requires explicit consideration of multiple paths without providing a "recipe" for locating all possible local transition states. Further, it is plausible that the position of the saddle point along any given reaction path could vary with potential if the local approach of using the static dipole moment and near-PZC polarizability are not sufficient to capture potential-dependent relaxation along the reaction coordinate. Collectively, we again emphasize that this approach then provides an upper bound on the barrier relative to the sampling of all possible reaction paths.

4.4. Sensitivity of electrification effects to unit-cell size

DFT-computed activation barriers calculated using periodic slab model can depend on the unit cell size. The capacitive correction term (Model 2a) provides an approach to extrapolate to constant workfunction, removing one source of unit cell size dependence. However, the polarized transition state will experience dipole–dipole repulsion with neighboring cells, and this repulsion could also lead to a reduced dipole moment resulting from the structural optimization or transition state search. To evaluate these cell-size effects, the same 2-water assisted proton transfer path was examined extending to 4x4 and 5x5 surface unit cells.

Fig. 8 plots the potential-dependent barrier for the same NH* reduction step across the 3 \times 3, 4 \times 4, and 5 \times 5 unit cells. Model 2b was used, avoiding polarizability calculations in the larger unit cells. A significant change in barrier is observed between the 3 \times 3 and 4 \times 4 unit cells, with the activation barrier at the PZC decreasing from 0.69 eV to 0.53 eV and the effective value of the symmetry coefficient also decreasing due to a larger dipole moment difference (-0.59 eÅ vs -0.72 eÅ) in the larger unit cell (Table S6). Changing the unit cell size from 4 \times 4 to 5 \times 5 makes a negligible difference relative to the 4 \times 4 cell, demonstrating that results have converged to the infinite cell size limit for the 4 \times 4 unit cell.

A unit cell size dependence on barriers (ie, a coverage interaction) is not surprising, especially considering the large surface dipole moments expected for ion transfer transition state structures and the size of the effective "adsorbate" when explicit water molecules accompany the small molecule adsorbate. These results are included to highlight an additional sensitivity of DFT calculated activation barriers for electrocatalytic reactions, both to make researchers in this area aware of the sensitivity and demonstrate the ease for which it is evaluated when using "traditional" constant charge DFT calculations and the extrapolation approach.

4.5. Sensitivity of activation barriers to double layer properties

Fig. 9 plots activation barriers using Model 2c and the same DFT results presented in Section 4.2, now varying the Helmholtz double layer $\frac{1}{2}$

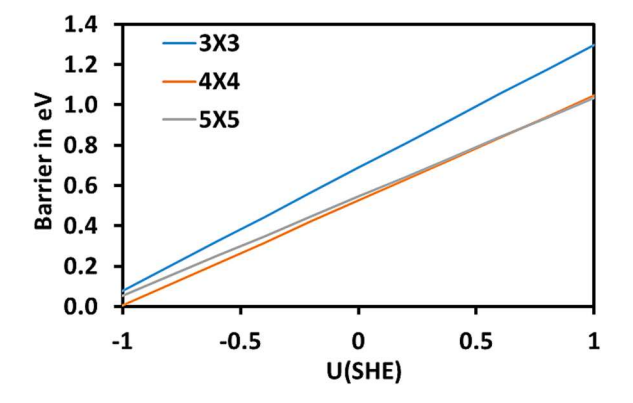


Fig. 8. Potential-dependent barriers for the reaction NH^* to NH_2^* on $\mathrm{Rh}(111)$ with 2 water molecules assisting, calculated with increasing unit cell sizes.

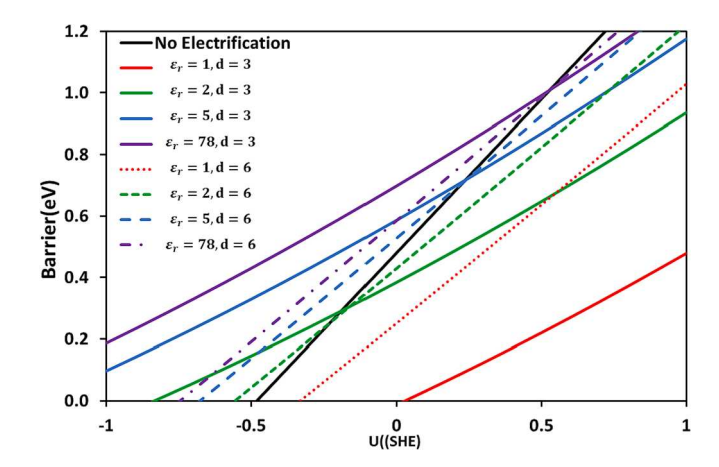


Fig. 9. Activation barriers as a function of electrode potential for NH* reduction to NH₂* on Rh(111) using different values for electrochemical double-layer properties. All curves are calculated using Model 2c and the same DFT results reported in Section 4.2, changing only the values of the dielectric permittivity (ε_r) and Helmholtz double-layer countercharge distance (d). The solid curves represent the Helmholtz double layer thickness of $d=3\text{\AA}$ and the dashed curve represents $d=6\text{\AA}$, with interfacial dielectric constant varying from 1(vacuum) to 78 (bulk water).

model parameters (ε_r and d). The table of 0th order (**c**), 1st order (**b**), and 2nd order coefficients (**a**) of the quadratic expressions are given in Table S8 along with the contributions of each term defined in Table 1.

Variations in interfacial dielectric constant have a significant effect on the potential-dependent activation barriers. The effect of dielectric constant arises mainly from the finite cell terms that are potential independent (Table S8), and, therefore, the interfacial dielectric permittivity has minimal effect on the symmetry factor. Barriers differ by $\sim\!0.8$ eV in changing the relative permittivity from 1 to 78.4, and even variation between 2 and 5 (a realistic range for relative permittivity near the metal surface) alters the barrier by over 0.2 eV.

Doubling the EDL counterion distance significantly alters both the activation barriers at the PZC and the symmetry factor. Solid and dashed curves for the same color in Fig. 7 contrast the thinner (d=3 Å) and thicker (d=6 Å) double-layers at the same value of ε_r . Further, the specific values of ε_r and d are important in dictating the activation barriers, rather than solely their ratio (ie., the specific capacitance or $\frac{\varepsilon}{d}$). Comparison of the solid red ($\varepsilon_r=1$ and d=3Å) and dashed green ($\varepsilon_r=2$ and d=6Å) curves in Fig. 9 shows significant variation in barrier.

The strong dependence of electrochemical activation barriers on the (typically unknown) interfacial dielectric permittivity and charge distribution is daunting, leaving large uncertainties in computed barriers. Regretfully, such uncertainties are inevitable given the inability of DFT methods to model the relevant time and length scales associated with the dynamic EDL structure. The compartmentalized extrapolation approach presented here makes these variations transparent, contrasting with methods to build a continuum double-layer model into the DFT calculation that include parameterization of these same properties. This also motivates attempts to examine such properties, whether via experiment or classical molecular dynamics simulations. The (potential-dependent) interfacial capacitance can be measured by electrochemical impedance spectroscopy to help bound reasonable EDL parameters, and can allow for the capacitance to be directly used in some terms (see Eq. (19) in our approach.

From a positive perspective, the results in Fig. 9 show a strong ability to alter electrochemical activation barriers, and thereby reaction rates, by altering EDL properties. The EDL provides an additional design parameter to impact electrocatalytic performance beyond changing the electrocatalyst design. Further, as discussed in the following section, the sensitivity of activation barriers to EDL properties can vary significantly

among different elementary reaction steps. This presents the potential to tune both activity and selectivity by tuning interfacial EDL properties.

4.6. Sensitivity of electrification effects to type of reaction

The magnitude of the most significant "corrections" to potential-dependent barriers beyond Model 1 depend strongly on the change in dipole moment along the reaction coordinate. The NH* reduction to NH $_2$ * elementary step has a significant change in dipole moment, as positive charge remained associated with the NH*-H $_5O_2^{\dagger}$ species at the transition state. Elementary reactions having a smaller change in dipole moment between the initial and transition state will show smaller "corrections" from the simplistic Model 1 approach, and therefore barriers that do not depend strongly on EDL properties.

We consider the elementary reaction of O* reduction to OH*, relevant to the oxygen reduction reaction, on the same surface Rh(111). We have considered only a one-water pathway for sampling the local TS for proton-shuttling. The surface normal dipole moments and polarizabilities along the reaction path are reported along with those for the NH* reduction to NH2* in Table S4. The transition state for O*-H bond formation is "late" such that electron transfer is nearly complete, and the change in dipole moment (-0.18eÅ) is small. Potential-dependent barriers estimates with different level of approximation (Model 2a-c) are shown in Fig. S8, with Fig. S7 showing the individual "correction" terms as a function of potenital. Fig. 10 illustrates potential-dependent barriers of O* reduction to OH* for various double-layer properties using Model 2c. The smaller sensitivity of the OH* formation barrier to EDL properties is clearly seen in contrasting Figs. 9 and 10. The dipole moment difference between the transition state and initial state provides a strong descriptor of whether a reaction rate constant will have a strong dependence on EDL properties.

5. Conclusion

A workflow for calculating potential-dependent electrochemical activation barriers for elementary steps involving ion–electron transfer was presented. The approach falls into the category of "extrapolation" approaches, using typical constant charge DFT calculations to extrapolate the potential dependence of the free energy of an adsorbed intermediate or transition state. The DFT energy, harmonic ZPVE and entropy corrections, surface normal dipole moment and polarizability of reactant and transition states are used as inputs to determine potential-dependent activation barriers. Interfacial electrochemical double-layer properties, specifically the dielectric permittivity and Helmholtz charge separation, are used as parameters in the "compartmentalized" model for barrier extrapolation as a function of electrode potential. The Supporting Information section details access to both Python code and a spreadsheet to utilize the Models presented herein.

The activation barrier for NH* reduction to $\mathrm{NH_2}^*$ on Rh(111) is significantly dependent on the specific solvation, long-range solvation, local reaction path, and interfacial dielectric properties. A virtue of the "compartmentalized" approach is that the dependence on each of these factors is transparent and quantifiable, though the typical uncertainty in these values leads to challenges in developing precise values from DFT calculations. We contrast this with DFT models that embed these choices into an DFT-continuum hybrid approach. The strong dependence of barriers on EDL properties presents an avenue to tune elementary reaction rates through varying solvent or electrolyte ion composition.

The interfacial dipole moment change along the reaction path is a robust predictor for whether an elementary activation barrier will strongly depend on interfacial EDL properties. NH* reduction is contrasted with O* reduction to demonstrate this difference.

We emphasize again that the specific transition state and reaction path considered for this reaction step is not necessarily the dominant, minimum energy path. A transition state is located, and its energy referenced to the "true" reactant state with the H^+ chemical potential

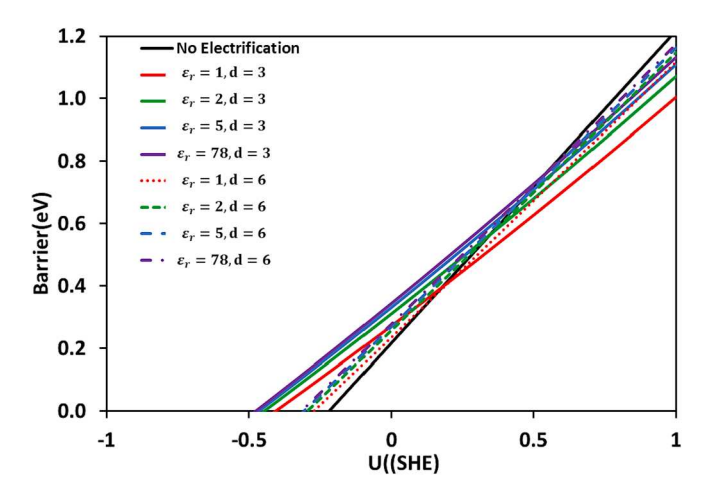


Fig. 10. Activation barriers calculated for O^* reduction to OH^* on Rh(111) using Model 2c and varying properties of the electrochemical double-layer.

taken in the bulk electrolyte. However, other paths may be envisioned with different trajectories of approach of the proton, through solvating water molecules, to the adsorbed species. A virtue of the approach presented is its relatively low computationally intensity – multiple trajectories can be explored, their DFT energies, workfunctions, and surface dipole moments determined, and the potential-dependent activation barriers considered to find the preferred path. As we considered only a single reaction path and transition state herein, it should be considered an "upper bound" on the barrier with the possibility that a lower energy path may exist.

Declaration of competing interest

The authors declare that they have no known competing financial interests or personal relationships that could have appeared to influence the work reported in this paper.

Data availability

A GitHub repository with code and structures has been prepared and the URL provided in the supplementary information statement of the manuscript.

Acknowledgements

The authors acknowledge funding from NSF-CBET 1939464. This work used Bridges at Pittsburgh Supercomputing Center and Expanse at San Diego Supercomputing Center through allocation CTS150057 from the Advanced Cyberinfrastructure Coordination Ecosystem: Services & Support (ACCESS) program [58], which is supported by National Science Foundation grants #2138259, #2138286, #2138307, #2137603, and #2138296.

Appendix A. Supplementary material

Supplementary data to this article can be found online at https://doi.org/10.1016/j.jcat.2024.115360. The GitHub repository can be found here: https://github.com/andrewjarkwahwong/dft-electrocatalysis-Janik

References

[1] S. Nitopi, E. Bertheussen, S.B. Scott, X. Liu, A.K. Engstfeld, S. Horch, B. Seger, I.E. L. Stephens, K. Chan, C. Hahn, J.K. Norskov, T.F. Jaramillo, I. Chorkendorff, Progress and perspectives of electrochemical CO(2) reduction on copper in aqueous electrolyte, Chem. Rev. 119 (2019) 7610–7672.

- [2] S.L. Foster, S.I.P. Bakovic, R.D. Duda, S. Maheshwari, R.D. Milton, S.D. Minteer, M. J. Janik, J.N. Renner, L.F. Greenlee, Catalysts for nitrogen reduction to ammonia, Nat. Catal. 1 (2018) 490–500.
- [3] L. Gong, N. Agrawal, A. Roman, A. Holewinski, M.J. Janik, Density functional theory study of furfural electrochemical oxidation on the Pt (1 1 1) surface, J. Catal. 373 (2019) 322–335.
- [4] L.O. Mark, N. Agrawal, A.M. Román, A. Holewinski, M.J. Janik, J.W. Medlin, Insight into the oxidation mechanism of furanic compounds on Pt (111), ACS Catal. 9 (2019) 11360–11370.
- [5] A.M. Román, J.C. Hasse, J.W. Medlin, A. Holewinski, Elucidating acidic electrooxidation pathways of furfural on platinum, ACS Catal. 9 (2019) 10305–10316.
- [6] Z.W. Seh, J. Kibsgaard, C.F. Dickens, I. Chorkendorff, J.K. Nørskov, T.F. Jaramillo, Combining theory and experiment in electrocatalysis: insights into materials design, Science 355 (2017) eaad4998.
- [7] N. Abidi, K.R.G. Lim, Z.W. Seh, S.N. Steinmann, Atomistic modeling of electrocatalysis: are we there yet? WIRES Comput. Mol. Sci. 11 (2020).
- [8] Q. Li, Y. Ouyang, S. Lu, X. Bai, Y. Zhang, L. Shi, C. Ling, J. Wang, Perspective on theoretical methods and modeling relating to electro-catalysis processes, Chem. Commun. (Camb) 56 (2020) 9937–9949.
- [9] R. Sundararaman, K. Schwarz, Evaluating continuum solvation models for the electrode-electrolyte interface: challenges and strategies for improvement, J. Chem. Phys. 146 (2017) 084111.
- [10] R. Sundararaman, K. Letchworth-Weaver, K.A. Schwarz, Improving accuracy of electrochemical capacitance and solvation energetics in first-principles calculations, J. Chem. Phys. 148 (2018) 144105.
- [11] J.K. Nørskov, J. Rossmeisl, A. Logadottir, L. Lindqvist, J.R. Kitchin, T. Bligaard, H. Jónsson, Origin of the overpotential for oxygen reduction at a fuel-cell cathode, J. Phys. Chem. B 108 (2004) 17886–17892.
- [12] S.A. Akhade, N.J. Bernstein, M.R. Esopi, M.J. Regula, M.J. Janik, A simple method to approximate electrode potential-dependent activation energies using density functional theory, Catal. Today 288 (2017) 63–73.
- [13] J.K. Nørskov, J. Rossmeisl, A. Logadottir, L. Lindqvist, J.R. Kitchin, T. Bligaard, H. Jonsson, Origin of the overpotential for oxygen reduction at a fuel-cell cathode, J. Phys. Chem. B 108 (2004) 17886–17892.
- [14] K.S. Exner, H. Over, Kinetics of electrocatalytic reactions from first-principles: a critical comparison with the ab initio thermodynamics approach, Acc. Chem. Res. 50 (2017) 1240–1247.
- [15] G. Rostamikia, S. Maheshwari, M.J. Janik, Elementary kinetics of nitrogen electroreduction to ammonia on late transition metals, Catal. Sci. Technol. 9 (2019) 174–181.
- [16] J. Greeley, T.F. Jaramillo, J. Bonde, I. Chorkendorff, J.K. Nørskov, Computational high-throughput screening of electrocatalytic materials for hydrogen evolution, Nat. Mater. 5 (2006) 909–913.
- [17] S. Wang, V. Vorotnikov, J.E. Sutton, D.G. Vlachos, Brønsted–Evans–Polanyi and transition state scaling relations of furan derivatives on Pd (111) and their relation to those of small molecules. ACS Catal. 4 (2014) 604–612.
- [18] G. Kumar, S.L.J. Lau, M.D. Krcha, M.J. Janik, Correlation of methane activation and oxide catalyst reducibility and its implications for oxidative coupling, ACS Catal. 6 (2016) 1812–1821.
- [19] L.D. Chen, M. Urushihara, K. Chan, J.K. Nørskov, Electric field effects in electrochemical CO2 reduction, ACS Catal. 6 (2016) 7133–7139.
- [20] T. Roman, A. Gross, Periodic density-functional calculations on work-function change induced by adsorption of halogens on Cu(111), Phys. Rev. Lett. 110 (2013) 156804.
- [21] F. Gossenberger, T. Roman, K. Forster-Tonigold, A. Gross, Change of the work function of platinum electrodes induced by halide adsorption, Beilst. J. Nanotechnol 5 (2014) 152–161.
- [22] K. Chan, J.K. Nørskov, Electrochemical barriers made simple, J. Phys. Chem. Lett. 6 (2015) 2663–2668.
- [23] J. Rossmeisl, E. Skúlason, M.E. Björketun, V. Tripkovic, J.K. Nørskov, Modeling the electrified solid-liquid interface, Chem. Phys. Lett. 466 (2008) 68–71.
- [24] N.G. Hörmann, O. Andreussi, N. Marzari, Grand canonical simulations of electrochemical interfaces in implicit solvation models, J. Chem. Phys. 150 (2019).
- [25] J.A. Herron, Y. Morikawa, M. Mavrikakis, Ab initio molecular dynamics of solvation effects on reactivity at electrified interfaces, Proc. Natl. Acad. Sci. 113 (2016) E4937–E4945.
- [26] M. Otani, I. Hamada, O. Sugino, Y. Morikawa, Y. Okamoto, T. Ikeshoji, Structure of the water/platinum interface—a first principles simulation under bias potential, PCCP 10 (2008) 3609–3612.
- [27] M. Otani, O. Sugino, First-principles calculations of charged surfaces and interfaces: a plane-wave nonrepeated slab approach, Phys. Rev. B 73 (2006) 115407.
- [28] Y. Sha, T.H. Yu, Y. Liu, B.V. Merinov, W.A. Goddard III, Theoretical study of solvent effects on the platinum-catalyzed oxygen reduction reaction, J. Phys. Chem. Lett. 1 (2010) 856–861.
- [29] Y. Sha, T.H. Yu, B.V. Merinov, P. Shirvanian, W.A. Goddard III, Oxygen hydration mechanism for the oxygen reduction reaction at Pt and Pd fuel cell catalysts, J. Phys. Chem. Lett. 2 (2011) 572–576.
- [30] K. Schwarz, R. Sundararaman, The electrochemical interface in first-principles calculations, Surf. Sci. Rep. 75 (2020) 100492.

- [31] S. Sakong, A. Groß, Water structures on a Pt(111) electrode from ab initio molecular dynamic simulations for a variety of electrochemical conditions, Phys. Chem. Chem. Phys. 22 (2020) 10431–10437.
- [32] G. Yang, S.A. Akhade, X. Chen, Y. Liu, M.-S. Lee, V.-A. Glezakou, R. Rousseau, J. A. Lercher, The nature of hydrogen adsorption on platinum in the aqueous phase, Angew. Chem. Int. Ed. 58 (2019) 3527–3532.
- [33] T. Cheng, H. Xiao, W.A. Goddard III, Full atomistic reaction mechanism with kinetics for CO reduction on Cu (100) from ab initio molecular dynamics freeenergy calculations at 298 K, Proc. Natl. Acad. Sci. 114 (2017) 1795–1800.
- [34] J.A. Gauthier, C.F. Dickens, H.H. Heenen, S. Vijay, S. Ringe, K. Chan, Unified approach to implicit and explicit solvent simulations of electrochemical reaction energetics, J. Chem. Theory Comput. 15 (2019) 6895–6906.
- [35] H.H. Heenen, J.A. Gauthier, H.H. Kristoffersen, T. Ludwig, K. Chan, Solvation at metal/water interfaces: an ab initio molecular dynamics benchmark of common computational approaches, J. Chem. Phys. 152 (2020).
- [36] K. Mathew, R. Sundararaman, K. Letchworth-Weaver, T. Arias, R.G. Hennig, Implicit solvation model for density-functional study of nanocrystal surfaces and reaction pathways, J. Chem. Phys. 140 (2014).
- [37] K. Chan, J.K. Nørskov, Potential dependence of electrochemical barriers from ab initio calculations, J. Phys. Chem. Lett. 7 (2016) 1686–1690.
- [38] G. Rostamikia, M.J. Janik, Borohydride oxidation over Au (111): a first-principles mechanistic study relevant to direct borohydride fuel cells, J. Electrochem. Soc. 156 (2008) B86.
- [39] G. Rostamikia, A.J. Mendoza, M.A. Hickner, M.J. Janik, First-principles based microkinetic modeling of borohydride oxidation on a Au (1 1 1) electrode, J. Power Sources 196 (2011) 9228–9237.
- [40] X. Nie, M.R. Esopi, M.J. Janik, A. Asthagiri, Selectivity of CO2 reduction on copper electrodes: the role of the kinetics of elementary steps, Angew. Chem. Int. Ed. 52 (2013) 2459–2462.
- [41] S.A. Akhade, R.M. Nidzyn, G. Rostamikia, M.J. Janik, Using Brønsted-Evans-Polanyi relations to predict electrode potential-dependent activation energies, Catal. Today 312 (2018) 82–91.
- [42] K. Mathew, V. Kolluru, S. Mula, S.N. Steinmann, R.G. Hennig, Implicit self-consistent electrolyte model in plane-wave density-functional theory, J. Chem. Phys. 151 (2019).
- [43] L. Fumagalli, A. Esfandiar, R. Fabregas, S. Hu, P. Ares, A. Janardanan, Q. Yang, B. Radha, T. Taniguchi, K. Watanabe, G. Gomila, K.S. Novoselov, A.K. Geim, Anomalously low dielectric constant of confined water, Science 360 (2018) 1339–1342.
- [44] B. Tran, Y. Zhou, M.J. Janik, S.T. Milner, Negative dielectric constant of water at a metal interface, Phys. Rev. Lett. 131 (2023) 248001.
- [45] P.E. Blöchl, Projector augmented-wave method, Phys. Rev. B 50 (1994) 17953–17979.
- [46] G. Kresse, J. Furthmüller, Efficient iterative schemes for ab initio total-energy calculations using a plane-wave basis set, Phys. Rev. B 54 (1996) 11169–11186.
- [47] G. Kresse, D. Joubert, From ultrasoft pseudopotentials to the projector augmentedwave method, Phys. Rev. B 59 (1999) 1758–1775.
- [48] J.P. Perdew, J.A. Chevary, S.H. Vosko, K.A. Jackson, M.R. Pederson, D.J. Singh, C. Fiolhais, Atoms, molecules, solids, and surfaces: applications of the generalized gradient approximation for exchange and correlation, Phys. Rev. B 46 (1992) 6671.
- [49] M. Methfessel, A. Paxton, High-precision sampling for Brillouin-zone integration in metals, Phys. Rev. B 40 (1989) 3616.
- [50] G. Henkelman, B.P. Uberuaga, H. Jónsson, A climbing image nudged elastic band method for finding saddle points and minimum energy paths, J. Chem. Phys. 113 (2000) 9901–9904.
- [51] G. Henkelman, H. Jónsson, A dimer method for finding saddle points on high dimensional potential surfaces using only first derivatives, J. Chem. Phys. 111 (1999) 7010–7022.
- [52] E. Wigner, J. Bardeen, Theory of the work functions of monovalent metals, Phys. Rev. 48 (1935) 84–87.
- [53] J.O.M. Bockris, S. Argade, Work function of metals and the potential at which they have zero charge in contact with solutions, J. Chem. Phys. 49 (1968) 5133–5134.
- [54] T.C. Leung, C.L. Kao, W.S. Su, Y.J. Feng, C.T. Chan, Relationship between surface dipole, work function and charge transfer: Some exceptions to an established rule, Phys. Rev. B 68 (2003) 195408.
- [55] B. Tran, S.T. Milner, M.J. Janik, Kinetics of acid-catalyzed dehydration of alcohols in mixed solvent modeled by multiscale DFT/MD, ACS Catal. 12 (2022) 13193–13206.
- [56] T. Pajkossy, D. Kolb, Double layer capacitance of Pt (111) single crystal electrodes, Electrochim. Acta 46 (2001) 3063–3071.
- [57] G. Valette, Double layer on silver single crystal electrodes in contact with electrolytes having anions which are slightly specifically adsorbed: Part II. The (100) face, J. Electroanal. Chem. Interfacial Electrochem. 138 (1982) 37–54.
- [58] T.J. Boerner, S. Deems, T.R. Furlani, S.L. Knuth, J. Towns, ACCESS: advancing innovation: NSF's advanced cyberinfrastructure coordination ecosystem: services & support, in: Practice and Experience in Advanced Research Computing, Association for Computing Machinery, Portland, OR, USA, 2023, pp. 173–176.